Nanotechnology

ACCEPTED MANUSCRIPT

Influence of experimental parameters on iron oxide nanoparticles properties synthesized by thermal decomposition: size and nuclear magnetic resonance studies

To cite this article before publication: Sarah Belaid *et al* 2018 *Nanotechnology* in press https://doi.org/10.1088/1361-6528/aaae59

Manuscript version: Accepted Manuscript

Accepted Manuscript is "the version of the article accepted for publication including all changes made as a result of the peer review process, and which may also include the addition to the article by IOP Publishing of a header, an article ID, a cover sheet and/or an 'Accepted Manuscript' watermark, but excluding any other editing, typesetting or other changes made by IOP Publishing and/or its licensors"

This Accepted Manuscript is **© 2018 IOP Publishing Ltd**.

During the embargo period (the 12 month period from the publication of the Version of Record of this article), the Accepted Manuscript is fully protected by copyright and cannot be reused or reposted elsewhere.
As the Version of Record of this article is going to be / has been published on a subscription basis, this Accepted Manuscript is available for reuse under a CC BY-NC-ND 3.0 licence after the 12 month embargo period.

After the embargo period, everyone is permitted to use copy and redistribute this article for non-commercial purposes only, provided that they adhere to all the terms of the licence https://creativecommons.org/licences/by-nc-nd/3.0

Although reasonable endeavours have been taken to obtain all necessary permissions from third parties to include their copyrighted content within this article, their full citation and copyright line may not be present in this Accepted Manuscript version. Before using any content from this article, please refer to the Version of Record on IOPscience once published for full citation and copyright details, as permissions will likely be required. All third party content is fully copyright protected, unless specifically stated otherwise in the figure caption in the Version of Record.

View the article online for updates and enhancements.

This content was downloaded from IP address 129.120.93.218 on 12/02/2018 at 23:14

Influence of experimental parameters on iron oxide nanoparticles properties synthesized by thermal decomposition: size and nuclear magnetic resonance studies

Sarah Belaïd[A], Dimitri Stanicki[A], Luce Vander Elst[A], Robert Muller[A, B], Sophie Laurent[A, B]

[A] *Department of General, Organic and Biomedical Chemistry, NMR and Molecular Imaging Laboratory, University of Mons, B-7000 Mons, Belgium*

[B] *Center for Microscopy and Molecular Imaging (CMMI), 6041 Gosselies, Belgium*

**Corresponding author: Sophie.laurent@umons.ac.be*

Accepted Manuscript

Abstract

The study of the experimental conditions to synthetize monodisperse iron oxide nanocrystals prepared from the thermal decomposition of iron (III) acetylacetonate in the presence of surfactants and reducing agent was carried out. The influence of temperature, synthesis time and surfactant amounts on nanoparticle properties are reported. This investigation combines the relaxometric characterization and size properties. The relaxometric behavior of nanomaterials depends on the selected experimental parameters. The synthesis of iron oxide nanoparticles with a high relaxivity and a high saturation magnetization can be obtained with a short reaction time at high temperature. Moreover, the influence of surfactant concentrations determines the optimal value in order to produce iron oxide nanoparticles with a narrow size distribution. The optimized synthesis is rapid, robust and reproductive, and produces nearly monodisperse magnetic nanocrystals.

Accepted Manuscript

1. Introduction

For the last decades, numerous groups reported the synthesis of iron oxide nanoparticles by a large panel of synthetic methods as coprecipitation [1-3], microemulsion [4-7], hydrothermal synthesis [8, 9], thermal decomposition [10-13], sol-gel [14-16] and polyol methods [17, 18]. Due to their interesting magnetic properties, iron oxide nanomaterials are essentially used in biomedical applications such as MRI contrast agents, nanocarriers for drug delivery and the cancer treatment by hyperthermia [19-22]. However, the magnetic properties of iron oxide nanoparticles are widely influenced by their physicochemical properties (size, size distribution, shape and surface nature) [23-26]. Therefore, the control of the size distribution is a real challenge for the researchers. It is reported that the production of magnetic nanoparticles with a controlled diameter and a better size distribution can be obtained by a high-temperature decomposition of iron inorganic precursors.

Rockenberger et al. [27] reported a general non hydrolytic method to synthesize transition metal oxide nanoparticles. In this method, iron(III) *N*-nitrosophenylhydroxylamine ($Fe(cup)_3$) was injected in octylamine solution under argon atmosphere at high temperature (250-300°C). After the synthesis, monodisperse iron oxide nanoparticles present a size range between 4 and 10 nm.

A few years later, Hyeon and co-workers [28] reported the production of monodisperse iron oxide nanoparticles. Nanoparticles were prepared from the thermal decomposition of iron(0) pentacarbonyl in a solution of octylether containing oleic acid to yield an iron oleate complex at low temperature. Then, the iron oleate solution was decomposed at high temperature (300°C) to obtain monodisperse iron nanoparticles by a controlled oxidation with trimethylamine as a mild oxidant, in order to form 11 nm-iron oxide nanoparticles.

Accepted Manuscript

Sun and co-workers [29] reported a high temperature reaction of iron(III) acetylacetonate with 1,2 hexadecanediol, oleic acid and oleylamine in a high boiling ether solution. In function of the nature and the boiling point of the solvent, particles of different sizes have been obtained: 4 nm particles are formed in presence of diphenylether and 6 nm particles are synthesized when dibenzylether is used. Numerous articles confirm the benefits of this synthetic approach by the use of several techniques such as transmission electron microscopy (TEM), X-ray diffraction (XRD) or/and vibrating sample magnetometry technique (VSM) [30, 31]. These reports essentially discussed the magnetic properties, the size and the size distribution of nanoparticles. The relaxometric behavior as a function of the modification of experimental parameters was poorly discussed in literature. Only few articles discuss the influence of experimental parameters on nuclear magnetic resonance properties [32-35]. Therefore, this article reports on the influence of experimental parameters of thermal decomposition method on the characteristics of the nanoparticles such as the size, the shape, the size distribution, the magnetic and the relaxometric properties. Moreover, the characterization was performed on the non-aqueous nanoparticle suspensions dispersed in n-heptane. This investigation defines an optimal protocol to obtain monodisperse iron oxide nanoparticles with a minimal synthesis time without the modification of standard size deviation.

2. Experimental section

2.1. Materials. Iron(III) acetylacetonate (97%), 1,2-hexadecanediol (90%), oleic acid (90%), oleylamine (70%), benzylether (99%) and iron standard for ICP-AES (TraceCerd©) were purchased from Sigma-Aldrich (Bornem, Belgium) and used as received. Ethanol (96%) and n-heptane (99%) were purchased from Acros Organic (Geel, Belgium) and used without purification.

2.2. Synthesis.

Accepted Manuscript

The iron oxide nanoparticles were prepared by a thermal decomposition of iron(III) acetylacetonate in dibenzylether in the presence of surfactants and reducing agent. The experimental parameters (time, temperature and surfactant concentration) were systematically modified for studying the effects of reaction factors on nanoparticles properties. Typically, solvent (dibenzylether), surfactants (oleic acid and oleylamine) and reducing agent (1,2-hexadecanediol) were added into a flask. The mixture was heated to the desired temperature (200°C, 250°C or 300°C) for 15 min and then iron(III) acetylacetonate diluted in dibenzylether was rapidly injected into the flask. The mixture was heated to a selected temperature and the heating period extended from 0 to 120 minutes during which a sample was taken every 30 minutes. Figure 1 shows the procedure approach to study the effect of time and temperature on the physicochemical properties of iron oxide nanoparticles with a 2:6 ratio between iron precursor and oleic acid amounts (standard condition).

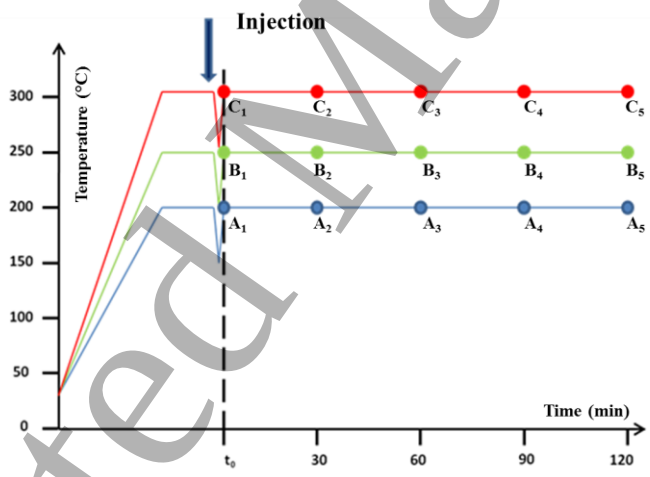

<u>Figure 1</u>: Heating protocol used to study the influence of the temperature and the time on the nanoparticle properties

The effect of surfactant amount was investigated with a mixture heated at 300°C during 30 minutes. The oleic acid and oleylamine (1:1) quantities were varied between 2 and 10

Accepted Manuscript

millimoles and other reaction parameters remained unchanged. The purification of aliquots consists in mixing the black mixture with ethanol in order to precipitate nanomaterials. Thanks to the use of magnetic separation, nanoparticles were isolated and the supernatant was discarded. The washing step was realized three times. Finally, the nanoparticles were dispersed in n-heptane for analysis.

To explore the influence of experimental parameters on the final physicochemical properties, different experiments were performed in which only one parameters (reaction time, temperature or surfactant amounts) was modified (table 1).

Table 1: Summary of the experimental parameters studied and the standard reaction factors used.

Parameters studied	
Heating time (min)	0, 30, 60, 90, 120
Heating temperature (°C)	200, 250, 300
Oleic acid and oleylamine (mmol)[a]	2, 3, 4, 6, 10
Standard parameters	
1,2-hexadecanediol (mmol)	10
Iron(III) acetylacetonate (mmol)	2
Dibenzylether (ml)	20

[a]The ratio between oleic acid and oleylamine amounts is equimolar and was kept constant for each run.

2.3. Characterization.

2.3.1. Nuclear Magnetic Resonance (NMR). The ^{1}H NMRD profiles was recorded using a Stelar Fast Field Cycling relaxometer (Mede, Italy). The system operates over a range of magnetic field extending from 0.25 mT to 0.94 T (0.01-40 MHz) at 37°C. T_1 and T_2 measurements were performed on a Bruker Minispec mq60 (Karlsrushe, Germany) working at a Larmor frequency of 60 MHz (1.41T) at 37°C. T_1 measurements were performed by an

Accepted Manuscript

inversion-recovery sequence (IR), which consists in an inversion (180°) pulse followed, after a delay t, by a 90° reading pulse. The measurement of T_1 consists thus in repeating this sequence with various inversion times, each sequence being separated from the next one by the recovery delay, RD (ideally equal to or larger than $5T_1$)..

T_2 is measured by the Carr–Purcell–Meiboom–Gill (CPMG) pulse sequence. In this sequence, a 90° pulse is followed by a series of 180° pulses, ideally covering the full decay of the signal.

2.3.2. Transmission Electron Microscopy (TEM). All TEM images were obtained using a Microscope Leo960E operating at an accelerating voltage of 60kV (Oregon, USA). The sample was prepared by placing a drop of diluted iron oxide nanoparticle suspensions on a carbon-coated copper grid. The liquid dries in air at room temperature.

2.3.3. Photon Correlation Spectroscopy (PCS). The PCS measurements were recorded on a Zetasizer NanoS from Malvern Instrument (Worcestershire, UK) using a detection angle of 173° and a red laser operated at a wavelength of 633 nm. The hydrodynamic diameters were measured on nanoparticle suspensions dispersed in n-heptane using the viscosity of n-heptane of 0.39 mPa.s at 25°C and the refractive index of iron oxide nanoparticles of 2.42.

2.3.4. Determination of iron content. The total amount of iron was determined by inductively coupled plasma-atomic emission spectroscopy (ICP-AES) using Jobin Yvon JY70$^+$ instrument (Longjumeau, France). All samples were prepared for analysis as follows: 0.2 ml of nanoparticle suspensions was added to 0.5 ml of concentrated nitric acid. The mixture was heated at 80°C during 30 minutes in a water bath. Distilled water was added to the mixture to reach a final volume of 5 ml.

Accepted Manuscript

2.3.5. X-ray diffraction (XRD). X-ray diffraction experiments were performed on a D5000 Siemens diffractometer using the Cu K_α radiation (λ=0.15406 nm). The scattering intensities were measured over an angular range of 20° < 2Θ< 80° for all samples. One measurement was recorded every 0.05° during 25 seconds. The measurements were recorded at room temperature.

2.3.6. Thermogravimetric analyses (TGA). The experiments were carried out on a TA Instruments Q500 (New Castle, United States) using Pt crucibles. The heating program is composed of an isotherm of 30 minutes at 100°C and then the samples were heated with a heating rate of 10°C min^{-1} until 800°C under a flow of nitrogen. 10-30 mg of iron oxide particle powders were used for analysis. For TGA coupled to a Fourier Transform Infra-Red, a Bruker Tensor 27 spectrometer equipped with a gas cell at 230°C was used.

3. Results and discussion

3.1. Nanoparticle formation by thermal decomposition

The thermal decomposition can be realized by two different methods: "heating-up" and "hot injection" methods for the production of nearly monodisperse nanoparticles. The heating-up process consists in progressive heating a pre-mixed solution of precursors, surfactants and solvent to a given temperature to initiate the nanoparticle clustering and growth [10, 36]. The hot injection method consists in achieving a fast homogeneous nucleation by the injection of reagents into a hot surfactant solution followed by a controlled growth phase. Both processes are based on the same formation mechanism [37] and are able to form nanoparticle suspensions with a narrow size distribution according to the control of the reaction parameters [38-40]. This work is focused on the hot injection method in which the synthesis mechanism

Accepted Manuscript

of nanoparticles is described by the well-known Lamer diagram [41]. This theory describes the formation of monodisperse nanoparticles thanks to the separation of the nucleation and growth phases. This can be achieved if: (i) nucleation and growth take place at different temperatures [29, 41] or (ii) nucleation and growth occurs with different rates [42].

After the injection of iron(III) acetylacetonate, the iron precursors are rapidly transformed to nuclei due to the precursor concentration increase and the subsequent supersaturation of the solution. Moreover, the temperature decreases, helping the burst nucleation of a majority of the iron initiators. Indeed, the growth rate slows down at lower temperatures. This step corresponds to the second stage in the Lamer diagram [41]. Then, the concentration of iron precursors simultaneous decreases with the rapid increase of temperature to higher values. This one induces the stop of the nucleation process. The crystal growth starts, inducing the size increase of the materials. Consequently, the hot injection method separates the nucleation and the growth processes by the use of different temperatures. This approach can be considered as a special case of Lamer theory in which the stage I is omitted.

To get further information about the thermal behavior of iron(III) acetylacetonate, a thermogravimetry analysis (TGA) was performed (Supporting information). The main weight loss (about 95%) is observed between 175°C and 300°C. This observation suggests the loss of acetylacetonate groups (acac). In order to identify the structure of residues, TGA coupling with infrared spectroscopy (TGA-IR) was performed (figure 2). The IR spectra measured by TGA-IR in gas phase (figure 2A) suggests the presence of acetylacetonate groups. Indeed, the IR spectrum at 200°C (figure 2B) indicates the presence of C=O bonds at 1730 cm^{-1} and is similar to the conventional Fourier transform infrared spectroscopy (FTIR) of 2,4-pentanedione (figure 2B) confirming that the temperature destabilizes iron(III) acetylacetonate complexes inducing the loss of these acac ligands.

Accepted Manuscript

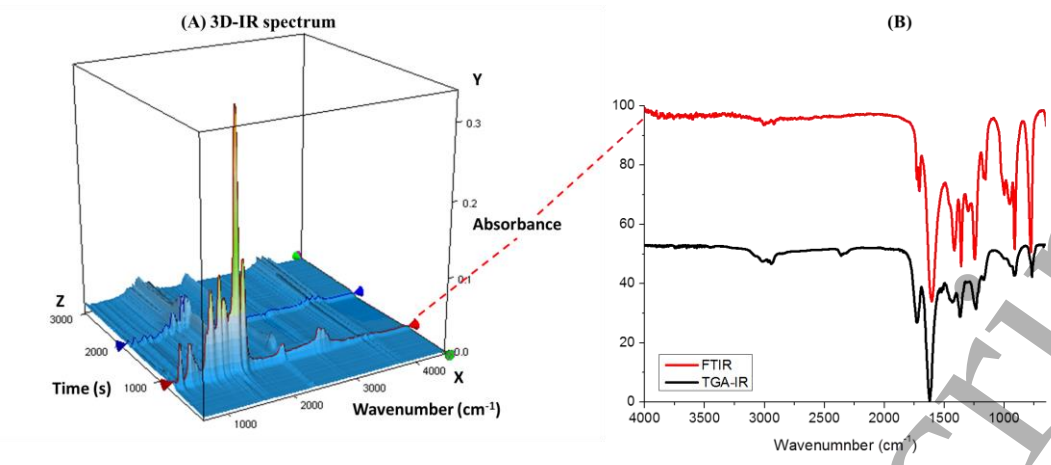

Figure 2: (A) IR-3D spectrum as a function of analysis time and temperature and (B) comparison of IR spectra between the iron(III) acetylacetonate residue measured by gas phase IR (black line) and the 2,4-pentanedione measured by FT-IR (red line).

Information available from the literature also reported the formation of other byproducts such as CO, CO_2, H_2, water, ketones and hydrocarbons with various chains [37, 43]. As a conclusion, these analyses give the temperature range required to decompose iron precursors that must be chosen between 175°C and 300°C.

3.2. Influence of heating temperature on nanoparticles properties

To study the effect of temperature, three samples A2, B2 and C2 heated at 200°C, 250°C and 300°C respectively, for 30 minutes with a ratio between iron precursors to oleic acid of 2:6. The nuclear magnetic relaxation properties of magnetic nanoparticles are generally obtained by the study of their nuclear magnetic resonance dispersion (NMRD) profiles (figure 3). These curves give the evolution of the proton longitudinal relaxivity (r_1) as a function of Larmor frequency.

Accepted Manuscript

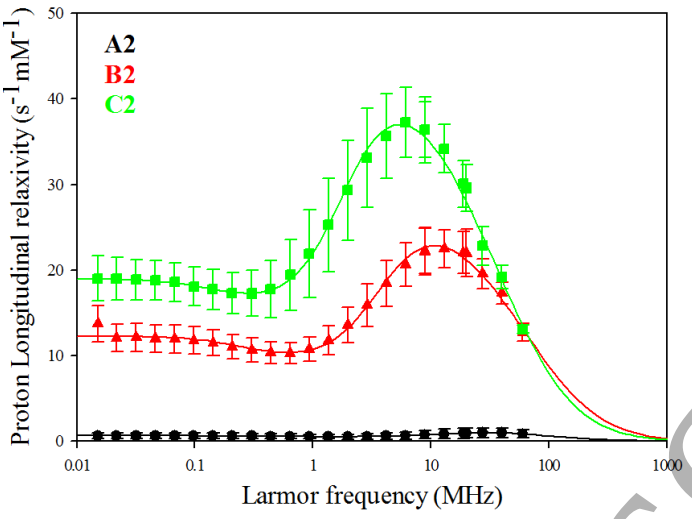

Figure 3: ^{1}H NMRD profiles of samples heated for 30 minutes at: 200°C (A2; black circle), 250°C (B2; red triangle) and 300°C (C2; green square). The continuous lines correspond to the fitting by the superparamagnetic relaxation theory (SPM).

The results indicate a marked difference between samples A2, B2 and C2. The general shape of these three NMRD profiles are similar and match well with the NMRD curves of superparamagnetic colloidal suspensions [44]. An increase of the temperature induces an increase of proton longitudinal relaxivity (r_1) at all values of Larmor frequencies. Moreover, the maximum longitudinal relaxivity (r_1^{max}) increases with synthesis temperature and its position moves toward lower proton Larmor frequencies, indicating an increase of particle size.

At lower Larmor frequencies (0.1-1MHz), a small dispersion is observed, indicating the presence of nanoparticles with a single crystal [45] and a low anisotropy energy [46]. Moreover, the longitudinal proton relaxivity at low frequencies increases when the samples are heated at higher temperatures, indicating the increase of anisotropy energy without the disappearance of the superparamagnetic property.

Accepted Manuscript

The experimental NMRD points of each sample were fitted using the superparamagnetic relaxation theory (SPM) [47, 48] adapted to non-aqueous suspensions of superparamagnetic nanoparticles (with a diffusion coefficient of n-heptane equal to 3.53 10^{-5} cm^2 s^{-1}) [49]. The relaxation models of superparamagnetic nanomaterials [47, 50] is based on the outer sphere model in which the theoretical parameters are extracted as NMRD diameter (d^{NMRD}) (corresponding to the shortest distance between the magnetic core and the solvent molecules), saturation magnetization (M_s) and Néel correlation times (τ_N) (see supporting information).

This relaxation model is defined as a dipolar interaction between the proton spins of the solvent molecules and the magnetic moment of superparamagnetic center in which the molecular interaction is modulated via the translational correlation time (τ_D) that depends on the relative diffusion and the distance between both centers (proton spin of solvent and magnetic moment of nanoparticles) [51]. The theoretical NMRD diameters and saturation magnetizations (table 2) increase with the temperature as predicted by the SPM theory. Indeed, similar effects can be observed for the samples heated at identical temperature but during various synthesis times (see supporting information). The d_{NMRD} is obtained from the fitting of the NMRD curves. The cristal size is obtained from the inflection point of high magnetic field component ($\omega\tau_D \sim 1$; $\tau_D = r^2/D$). The low particle size and the high dispersity of the sample may explain the high $d_{NMRD.}$ The diameter d^{XRD} have been estimated from Scherrer formula. It not always gives a real crystallite size value. The shape constant (k = 0.89 ~0.9) is used for spherical particles, so the cristallite have to be spherical, which is not the case for all our samples. The Ms has been obtained from from the fitting of the NMRD curves and is based on the classical outersphere relaxation model. The resulting low Ms values are probably the consequence of a deep and extended coating on the surface hindering the

Accepted Manuscript

approach of the stericaly imposing solvent molecules (i.e. heptane) at the nearby of the magnetic core.

Table 2: Summary of the experimental parameters and the results obtained for the study of the influence of time and temperature.

Experimental details				Diameter (nm)			PDI	M_s
Sample	**Temperature (°C)**	**Time (min)**	**Fe:Surf**	d^{NMRD}	d^{XRD}	d^{TEM}		**($A.m^2$/Kg of iron)**
A2	200	30	2:6	9.0	3.0	4.3±1.7	1.5	13.4
B2	250	30	2:6	9.5	6.5	5.7±1.8	1.4	49.5
C2	300	30	2:6	12.3	5.4	8.0±2.4	1.3	47.5
C1	300	0	2:6	9.6	/	7.0±2.0	1.3	42.6
C3	300	60	2:6	12.4	/	8.4±2.7	1.3	46.7
C4	300	90	2:6	12.1	/	8.2±2.3	1.3	47.5
C5	300	120	2:6	11.5	6.0	9.4±2.5	1.2	48.7

As a conclusion, the heating of reaction mixture at high temperature induces an increase of longitudinal relaxivity as well as an increase of crystal size. In order to obtain nanoparticle suspensions with a high relaxivity, it is essential to select a temperature larger than 200°C as predicted previously by the TGA analysis of iron(III) acetylacetonate. In a previous work, we have also reported [48] the evolution of NMR behaviors of compounds during the thermal decomposition process. A large difference between the NMRD profiles of aliquots taken at low temperature and at high temperature was observed. This can be due to an increase of nanoparticle size.

In order to investigate the temperature influence on size properties, XRD and TEM were used to characterize the crystalline nature and the core size (figure 4B). X-ray diffraction analysis gives the size of the crystal as well as a qualitative information on the crystallinity. For this, XRD diameter (d^{xrd}) was estimated from the Scherrer formulation [53]. The position and relative intensity of all peaks match well with standard XRD data of the structure of iron oxide powders (maghemite or magnetite). The XRD peak intensity of each sample increases

Accepted Manuscript

with heating temperature. Sample C2 (heated at 300°C) exhibits peaks with higher intensities than samples A2 (heated at 200°C) and B2 (heated at 250°C) for the predominant lattice face of (311), (511) and (440). Sample heated at 200°C (sample A2) does not seem to be crystalline. On the contrary, when the temperature is increased to 250°C or 300°C, the characteristic XRD peaks of magnetite or maghemite clearly appear, demonstrating the presence of crystalline nanoparticles. Moreover, the narrow width of these XRD peaks shows that these samples (B2 and C2) exhibit a crystalline proportion much higher than samples heated at 200°C (samples A2).

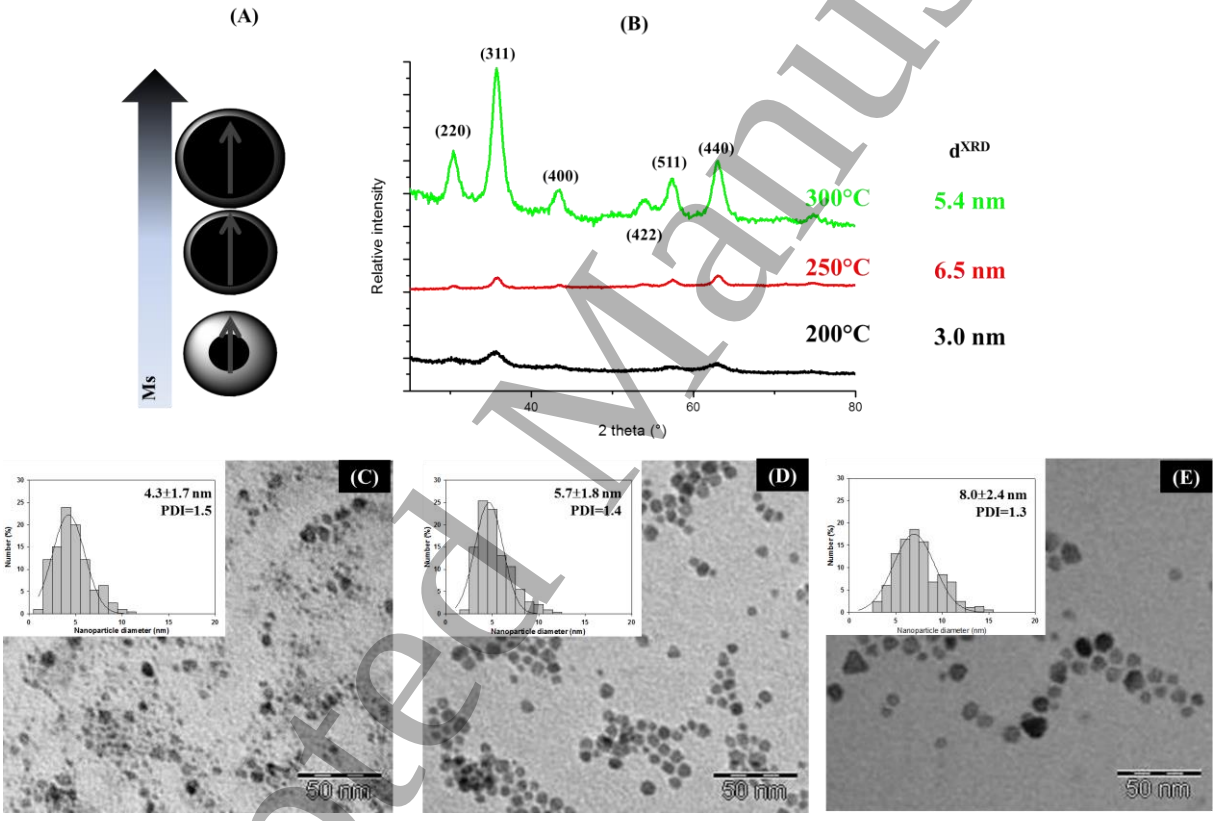

<u>Figure 4</u>: (A) Schematic illustration of size evolution and saturation magnetization, (B) X-ray diffraction patterns of samples heated for 30 minutes at: 200°C (sample A2: black line), 250°C (sample B2: red line) or 300°C (sample C2: green line) and TEM images of (C) sample A2, (D) sample B2 and (E) sample C2.

Accepted Manuscript

To complete the size characterization, transmission electron microscopy was used to study the morphology of each sample (figure 4). After the diameter measurement of a nanoparticle set (around 600-1000 of particles/ sample), the statistical treatment of the size histograms was fitted by a Gaussian function. The TEM diameter, the standard deviation and the polydispersity index (PDI) were calculated. It is observed that TEM diameters increase with reaction temperature, whereas, PDI tends to decrease (table 2).

These data agree with the NMRD results, showing that sample A2 exhibits a low value of calculated saturation magnetization. At 200°C, the synthesis temperature is thus not sufficient to form nanoparticles with a high crystallinity level. At higher temperatures, the TEM diameter increases and is in good agreement with the results obtained by NMRD and XRD measurements. The comparison between NMR and size properties shows a good correlation and the difference observed between both TEM and XRD diameters can be related to the values of saturation magnetization. According to several reported works, the evolution of saturation magnetization is due to the growth of crystal size [8, 25, 54]. Therefore, the increase of the crystallinity degree and the nanoparticle size induces high impacts on the relaxometry properties of iron oxide nanoparticles.

3.3. Influence of heating time on nanoparticle properties.

The heating time effect is also an important factor influing on the nanoparticle properties. In this part, the study was focused on the NMR and size characterizations of the samples heated at 300°C (samples C1 to C5) as a function of heating time. As shown above, the samples heated at higher temperature exhibit a much higher relaxivity and crystallinity level; therefore, we focused on these samples. The solution was synthesized with the same ratio between iron precursor and surfactants (2:6). The heating time varied from 0 minutes to 120 minutes, an

Accepted Manuscript

aliquot was taken every 30 minutes during the synthesis process and other reaction factors were unchanged.

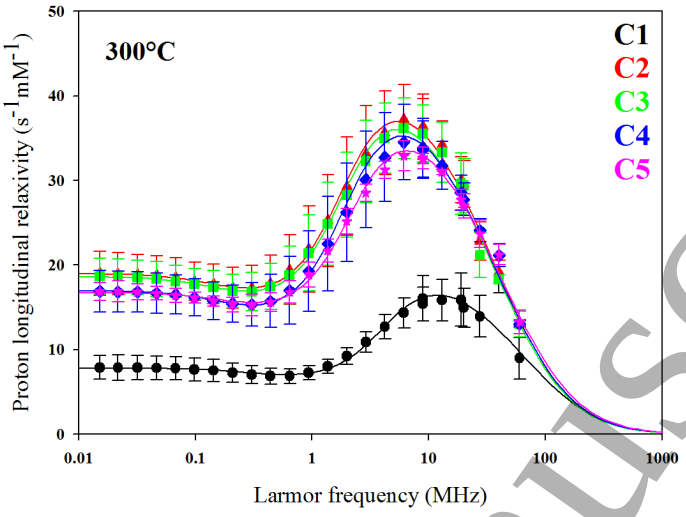

Figure 5: ^{1}H relaxation profiles, recorded at 37°C in n-heptane, for samples heated at 300°C during: 0 min (C1; black circle), 30 min (C2; red triangle up), 60 min (C3; green square), 90 min (C4; blue diamond) and 120 min (C5; pink triangle down).

Figure 5 shows the time influence on NMRD profiles of aliquots heated at 300°C. NMRD profile of sample C1 exhibits a proton longitudinal relaxivity much lower than the other samples over the whole range of proton Larmor frequencies. In addition, NMRD profiles of samples C2 to C5 exhibit analogous values of longitudinal relaxivities. The maximum longitudinal relaxivity remains at the same Larmor frequency (around 10 MHz). It seems thus that the heating time slightly influences the NMR properties of nanoparticles. As a result, the influence of reaction temperature is much more important than the heating time on relaxometric properties. All NMRD profiles were fitted with SPM theory to extract the NMRD parameters (table 2). As depicted in table 2, NMRD diameter of sample C1 (corresponding to sample taken at initial reaction time) is smaller than for the other samples. A significant increase of NMRD values (d^{NMRD}, M_S and τ_N) is observed between samples C1

Accepted Manuscript

and C2. However, similar values are observed for samples C2 to C5. An increase of the nanoparticle diameter is related to an increase of saturation magnetization. As a result, the heating time slightly influences the relaxometry parameters. In order to confirm these observations, TEM were performed on the samples heated at 300°C (Supporting informations). It was observed that TEM diameter tends to slightly increase as a function of the heating time when the reaction mixture is heated at 300°C (figure 6) whereas PDI slowly decreases with the heating time.

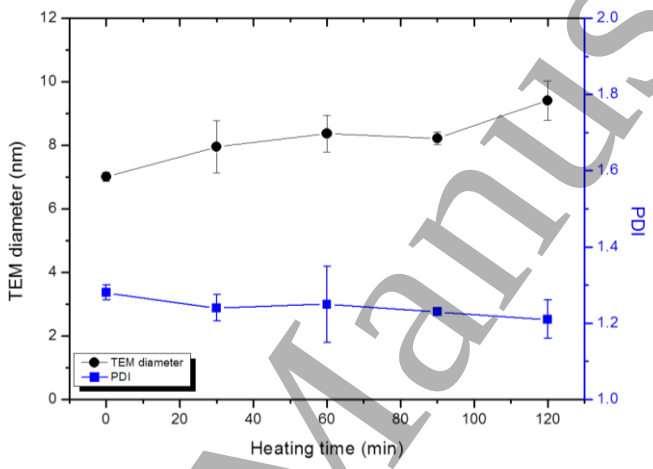

<u>Figure 6</u>: Heating time effect on the TEM diameter and the polydispersity index (PDI) of samples heated at 300°C.

Data discussed in the literature are sometimes contradictory concerning the influence of heating time on the properties of iron oxide nanoparticles synthesized by thermal decomposition. For example, Schladt et al. [55] reported that the nanoparticle size increases with heating time whereas the PDI values decrease. These data agree well with our results. However, Maity et al. [56] reported the deterioration of polydispersity index with the heating time. In our case, a low influence of reaction times is observed on nanoparticle size, size distribution, magnetic and relaxometric properties. Consequently, in order to form a

Accepted Manuscript

nanoparticle suspension with high performance, in terms of relaxivities and magnetization, the optimal temperature seems to be of 300°C with a minimal reaction time of 30 minutes.

In order to select the optimal experimental parameters, the relationship between the reaction time and the synthesis temperature was investigated. Figure 7 shows the influence of synthesis time and temperature on the longitudinal relaxivity (**a**), transversal relaxivity (**b**) and their ratio (**c**) measured at a Larmor frequency of 60 MHz and at 37°C. The magnetic properties are illustrated with the values of saturation magnetization (**d**) of each sample extracted from the fitting of NMRD profiles according to the superparamagnetic relaxation theory.

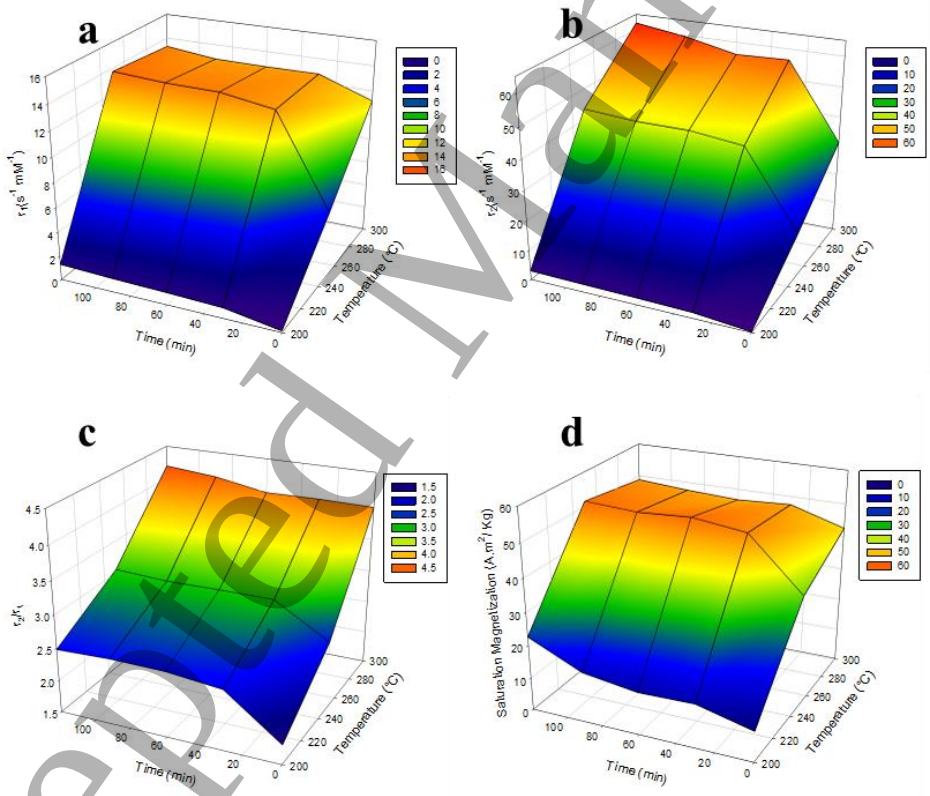

Figure 7: Influence of reaction time and temperature on nanoparticle properties: (a) longitudinal relaxivity r_1, (b) transversal relaxivity r_2, (c) ratio between transversal and

Accepted Manuscript

longitudinal relaxivities r_2/r_1 and (d) saturation magnetization. The relaxometric values were measured at 60 MHz and 37°C.

Figure 7a shows the evolution of longitudinal relaxivity as a function of reaction time and temperature. At a fixed temperature, the r_1 remains nearly constant between 30 and 120 minutes, whereas, at identical time, the value of r_1 progressively increases when the synthesis temperature changes from 200°C to 250°C and remains constant at 300°C. For the transversal relaxivity (figure 7b), an increase is observed between 250°C and 300°C. The saturation magnetization (figure 7d) behaves similarly to r_1.

Figure 7c shows the ratio between the longitudinal and transversal relaxivities (r_2/r_1) at 60 MHz and at 37°C. The ratio strongly increases when the temperature increases, since r_2 increases more and faster than r_1. This observation can be explained by an increase of nanoparticle size and crystallinity level as shown by TEM images and by X-ray diffraction patterns.

At high temperature, the decomposition of acetylacetonate complexes is easier. Therefore, the formation of the primary iron species followed by the nanoparticle growth can take place. At 300°C, a mass transfer of primary species on nanoparticle surface can be facilitated in favor of the crystal growth.

3.4. Influence of surfactant concentrations

During the last decades, numerous works reported the influence of surfactants during the synthetic process [25, 56, 57]. The surfactants can play two roles: (i) they sterically avoid agglomeration and (ii) they play an active role in the nanoparticle growth. In our case, iron oxide nanoparticles are formed by the thermal decomposition of iron(III) acetylacetonate in the presence of oleic acid (OA), oleylamine and 1,2-hexadecanediol in dibenzylether. Oleic

Accepted Manuscript

acid is frequently used in thermal decomposition process due to the presence of a double bond giving a better steric stabilization. Yin et al. [58] reported that oleic acid influences the temperature decomposition of iron precursors and also affects the nanoparticle size. However, the results reported about the surfactant influence are not always clear. Although the influence of oleic acid is extensively discussed, the data found in the literature are sometimes contradictory. Some authors assumed that the nanoparticle size tends to increase with the surfactant concentration, whereas other research groups reported the inverse tendency [42, 58-619].

Consequently, the optimal ratio of oleic acid to iron precursor must be determined for the production of monodisperse nanoparticles. To this purpose, the reactant solutions were heated at 300°C for 30 minutes. As described previously, these conditions are the temperature and the reaction time required to obtain iron oxide nanoparticles with optimal magnetic and relaxometric properties.

Different surfactant concentrations (oleic acid and oleylamine) were investigated (samples D1 to D5; table 3). The concentration of iron precursors as well as 1,2-hexadecanediol and dibenzylether did not change in these experiments. The ratio between both surfactants, oleic acid and oleylamine, is equimolar. Indeed, in the literature, it is demonstrated that an equivalent concentration of both surfactants form small nanoparticles with a narrow size distribution [62].

Table 3: Summary of the experimental parameters and the results obtained for the study of the influence of surfactant.

Experimental details				Diameter (nm)			PDI
Sample	**Temperature (°C)**	**Time (min)**	**Fe:Surf**	d^{PCS}	d^{XRD}	d^{TEM}	
D1	300	30	2:2	9.9±2.6	6.0	6.1±0.9	1.1
D2	300	30	2:3	9.7±2.5	6.4	9.4±2.6	1.2
D3	300	30	2:4	9.0±2.2	5.6	8.4±1.8	1.2

Accepted Manuscript

D4	300	30	2:6	9.5±2.3	5.5	8.0±2.0	1.2
D5	300	30	2:10	9.5±2.3	5.7	7.3±2.1	1.3

To study the size properties, three characterization techniques (PCS, XRD and TEM) were used. PCS data show similar values of hydrodynamic diameter for each sample (table 3). Therefore, the surfactant amount does not seem to influence the hydrodynamic diameter. Similarly, XRD analysis (Supporting informations) shows similar spectra, correlated to the typical XRD spectra of the magnetite or maghemite. The calculated diameters (from (311) XRD peaks) exhibit similar values (around 5.5 and 6.5 nm) for each sample. After the statistical treatments (with a nanoparticle number of 600-1000), the evolution of TEM diameters and the polydispersity index (figure 8) shows that the nanoparticle size increases when oleic acid content increases from to 2 mmol (sample D1) to 3 mmol (sample D2), and then decreases. On the other hand, the size dispersity tends to increases when increasing the surfactant concentration.

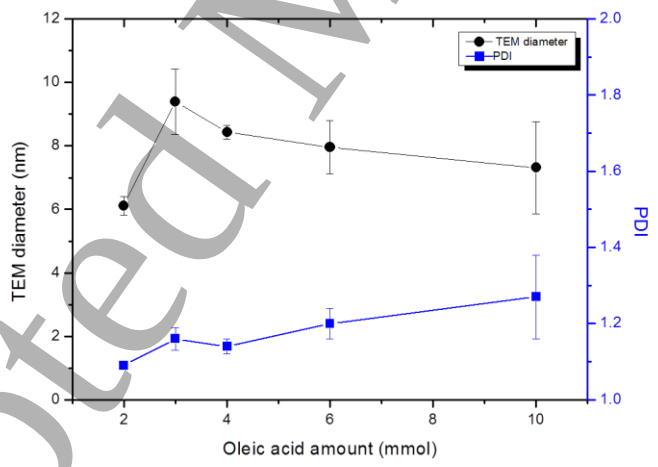

<u>Figure 8</u>: Evolution of TEM diameter and polydispersity index (PDI) as a function of oleic acid amount.

Accepted Manuscript

As shown in figures 8 and 9, the size distribution becomes broader for samples D2 to D5 (corresponding to surfactant amount between 3 and 10 mmol). When the surfactant and iron precursor amounts are equimolar (sample D1: 2 mmol) , the particles are spherical, uniform and exhibit a smaller size compared to other samples.

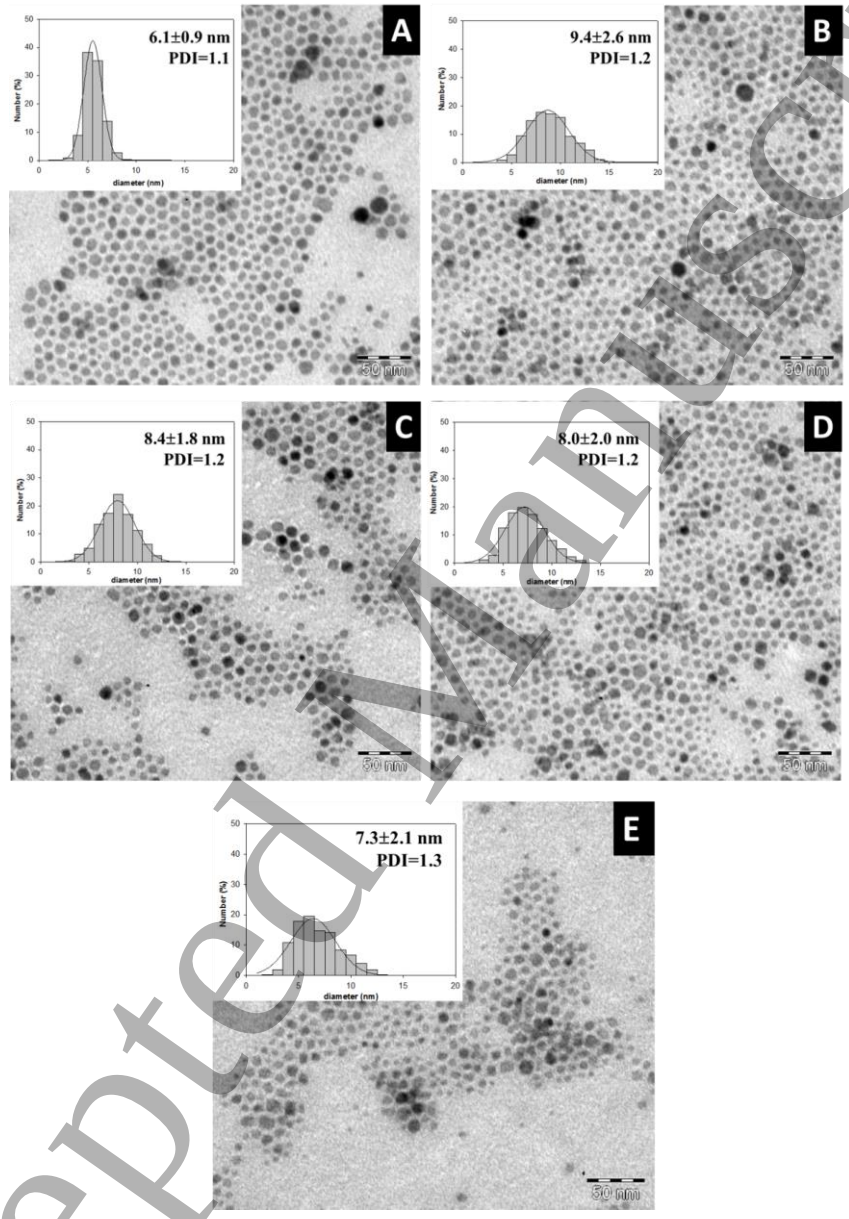

<u>Figure 9</u>: TEM images and their size histograms of the samples heated at 300°C during 30 minutes with a surfactant amount of: (A) 2mmol, (B) 3mmol, (C) 4mmol, (D) 6mmol and (E) 10 mmol.

Accepted Manuscript

For the thermal decomposition of iron (III) acetylacetonate in the presence of oleic acid, oleylamine and 1,2-hexadecanediol, contradictory results have been reported. Vargas et al. [63] stated that the nanoparticle diameter continually decreases with the increase of oleic acid amount. On the other hand, Meledandri et al. [64] observed the inverse situation in which the particle size decreases with surfactant quantity as shown by several characterizations. Finally, Bronstein et al. [65] reported that the crystal size increases and then decreases with oleic acid concentration. In the present work, monodisperse nanoparticles were obtained when the surfactant amount is equal to 2 mmol while larger amounts of oleic acid induce a broadening of the size distribution. Moreover, this optimized protocol is reproducible (as shown in supporting information by NMRD profiles and VSM curves).

Accepted Manuscript

4. Conclusions

The control of the size distribution is a major challenge which was fulfilled in this study for the production of monodisperse iron oxide nanoparticles. The influence of reaction factors (temperature, time and surfactant concentration) was investigated in order to define their impact on nanoparticle properties and to determine optimal experimental parameters for the production of monodisperse iron oxide nanoparticles. The present investigation showed that the reaction temperature and the surfactant concentration have larger effects than the reaction time. The optimized experimental protocol could be identified as follows: the reaction solution should be heated at 300°C during a minimum of 30 minutes with an equimolar Fe:OA ratio (2:2)., The optimized experimental protocol allowed a fast and reproducible synthesis of monodisperse iron oxide nanoparticles (6 nm).

Acknowledgements

This work was supported by the ARC Programs of the French Community of Belgium and the FNRS (Fond National de la Recherche Scientifique). The support and sponsorship provided by COST Actions (TD1004 and TD1402), ENCITE and of the EMIL programs are acknowledged. S. Belaïd is grateful to the FRIA (Fonds de la Recherche Industrielle et Agricole) for its financial support. The authors thank the laboratories of Prof. D. Nonclercq for the use of TEM, of Prof Y. Gossuin for the VSM measurements and of Prof. Dubois for TGA data.

Accepted Manuscript

5. References

1. Li J, Wang S, Shi X, Shen M. (2017) Aqueous-phase synthesis of iron oxide nanoparticles and composites for cancer diagnosis and therapy. Adv. Colloid Interface Sci. S0001-8686 (17) : 30069-6.

2. Pereira, C., Pereira, A.M., Fernandes, C., Rocha, M., et al. (**2012**). Superparamagnetic MFe_2O_4 (M = Fe, Co, Mn) nanoparticles: tuning the particle size and magnetic properties through a novel one-step coprecipitation route. Chemistry of Materials 24(8): 1496-1504.

3. Bhandari R, Gupta P, Dziubla T, Hilt JZ. **(2016)** Single step synthesis, characterization and applications of curcumin functionalized iron oxide magnetic nanoparticles. Mater Sci Eng C Mater Biol Appl. 67: 59-64.

4. Chin, A.B. and Yaacob, I.I. (**2007**). Synthesis and characterization of magnetic iron oxide nanoparticles via w/o microemulsion and Massart's procedure. Journal of Materials Processing Technology 191(1–3): 235-237.

5. Okoli C, Sanchez-Dominguez M, Boutonnet M, Järås S, Civera C, Solans C, Kuttuva GR. (2012) Comparison and functionalization study of microemulsion-prepared magnetic iron oxide nanoparticles. Langmuir. 28(22): 8479-85.

6. Nassar, N. and Husein, M. (**2006**). Preparation of iron oxide nanoparticles from $FeCl_3$ solid powder using microemulsions. Physica Status Solidi (a) 203(6): 1324-1328.

7. Santra, S., Tapec, R., Theodoropoulou, N., Dobson, J., et al. (**2001**). Synthesis and characterization of silica-coated iron oxide nanoparticles in microemulsion: the effect of nonionic surfactants. Langmuir 17(10): 2900-2906.

8. Ge, S., Shi, X., Sun, K., Li, C., et al. (**2009**). Facile hydrothermal synthesis of iron oxide nanoparticles with tunable magnetic properties. The Journal of Physical Chemistry C 113(31): 13593-13599.

9. Takami, S., Sato, T., Mousavand, T., Ohara, S., et al. (**2007**). Hydrothermal synthesis of surface-modified iron oxide nanoparticles. Materials Letters 61(26): 4769-4772.

10. Chen, Z. (**2012**). Size and shape controllable synthesis of monodisperse iron oxide nanoparticles by thermal decomposition of iron oleate complex. Synthesis and Reactivity in Inorganic, Metal-Organic, and Nano-Metal Chemistry 42(7): 1040-1046.

11. Lassenberger A, Grünewald TA, van Oostrum PDJ, Rennhofer H, Amenitsch H, Zirbs R, Lichtenegger HC, Reimhult E. **(2017)** Monodisperse Iron Oxide Nanoparticles by Thermal Decomposition: Elucidating Particle Formation by Second-Resolved in Situ Small-Angle X-ray Scattering. Chem Mater. 29(10): 4511-4522.

Accepted Manuscript

12. Roca, A.G., Morales, M.P., O'Grady, K. and Serna, C.J. (**2006**). Structural and magnetic properties of uniform magnetite nanoparticles prepared by high temperature decomposition of organic precursors. Nanotechnology 17(11): 2783.

13. Unni M, Uhl AM, Savliwala S, Savitzky BH, Dhavalikar R, Garraud N, Arnold DP, Kourkoutis LF, Andrew JS, Rinaldi C. **(2017)** Thermal Decomposition Synthesis of Iron Oxide Nanoparticles with Diminished Magnetic Dead Layer by Controlled Addition of Oxygen. ACS Nano. 11(2): 2284-2303.

14. Richard S, Eder V, Caputo G, Journé C, Ou P, Bolley J, Louedec L, Guenin E, Motte L, Pinna N, Lalatonne Y. **(2016)** USPIO size control through microwave nonaqueous sol-gel method for neoangiogenesis T2 MRI contrast agent. Nanomedicine (Lond).

15. Leonardi SG, Mirzaei A, Bonavita A, Santangelo S, Frontera P, Pantò F, Antonucci PL, Neri G. **(2016)** A comparison of the ethanol sensing properties of α-iron oxide nanostructures prepared via the sol-gel and electrospinning techniques. Nanotechnology. 27(7): 075502. doi: 10.1088/0957-4484/27/7/075502.

16. Xu, J., Yang, H., Fu, W., Du, K., et al. (**2007**). Preparation and magnetic properties of magnetite nanoparticles by sol–gel method. Journal of Magnetism and Magnetic Materials 309(2): 307-311.

18. Liu, H.-L., Ko, S.P., Wu, J.-H., Jung, M.-H., et al. (**2007**). One-pot polyol synthesis of monosize PVP-coated sub-5nm Fe_3O_4 nanoparticles for biomedical applications. Journal of Magnetism and Magnetic Materials 310(2, Part 3): e815-e817.

19. Bonvin D, Bastiaansen JAM, Stuber M, Hofmann H, Mionić Ebersold M. **(2017)** Folic acid on iron oxide nanoparticles: platform with high potential for simultaneous targeting, MRI detection and hyperthermia treatment of lymph node metastases of prostate cancer. Dalton Trans. 46(37): 12692-12704.

20. Ingrid Hilger, W.A.K. (**2012**). Iron oxide-based nanostructures for MRI and magnetic hyperthermia. Nanomedecine 7(9): 1443-1459.

21. Reddy, L.H., Arias, J.L., Nicolas, J. and Couvreur, P. (**2012**). Magnetic nanoparticles: design and characterization, toxicity and biocompatibility, pharmaceutical and biomedical applications. Chemical Reviews 112(11): 5818-5878.

22. Wahajuddin, A.S. (**2012**). Superparamagnetic iron oxide nanoparticles: magnetic nanoplatforms as drug carriers. International Journal of Nanomedicine 7(1): 3445-3471.

23. Bittova, B., Poltierova-Vejpravova, J., Roca, A.G., Morales, M.P., et al. (**2010**). Effects of coating on magnetic properties in iron oxide nanoparticles. Journal of Physics: Conference Series 200(7): 072012.

24. Gao, G., Liu, X., Shi, R., Zhou, K., et al. (**2010**). Shape-controlled synthesis and magnetic pproperties of monodisperse Fe_3O_4 nanocubes. Crystal Growth & Design 10(7): 2888-2894.

Accepted Manuscript

25. Guardia, P., Labarta, A. and Batlle, X. (**2010**). Tuning the size, the shape, and the magnetic properties of iron oxide nanoparticles. The Journal of Physical Chemistry C 115(2): 390-396.

26. Smolensky, E.D., Park, H.-Y.E., Berquó, T.S. and Pierre, V.C. (**2011**). Surface functionalization of magnetic iron oxide nanoparticles for MRI applications – effect of anchoring group and ligand exchange protocol. Contrast Media & Molecular Imaging 6(4): 189-199.

27. Rockenberger, J., Scher, E.C. and Alivisatos, A.P. (**1999**). "A new nonhydrolytic single-precursor approach to surfactant-capped nanocrystals of transition metal oxides." Journal of the American Chemical Society 121(49): 11595-11596.

28. Hyeon, T., Lee, S.S., Park, J., Chung, Y., et al. (**2001**). "Synthesis of highly crystalline and monodisperse maghemite nanocrystallites without a size-selection process." Journal of the American Chemical Society 123(51): 12798-12801.

29. Sun, S., Zeng, H., Robinson, D.B., Raoux, S., et al. (**2003**). "Monodisperse MFe_2O_4 (M = Fe, Co, Mn) nanoparticles." Journal of the American Chemical Society 126(1): 273-279.

30. Lak, A., Ludwig, F., Grabs, I.-M., Garnweitner, G., et al. (**2010**). "Influence of synthesis parameters on magnetization and size of iron oxide nanoparticles." AIP Conference Proceedings 1311(1): 224-230.

31. Miguel-Sancho, N., Bomati-Miguel, O., Roca, A.G., Martinez, G., et al. (**2012**). "Synthesis of magnetic nanocrystals by thermal decomposition in glycol media: effect of process variables and mechanistic study." Industrial & Engineering Chemistry Research 51(25): 8348-8357.

32. Gossuin, Y., Serhan, Z., Sandiford, L., Henrard, D., et al. **(2016)**. "Sample Shuttling Relaxometry of Contrast Agents: NMRD Profiles above 1 T with a Single Device." Appl Magn Reson. 47: 237-246.

33. Basini, M., Orlando, T., Arosio, P., Casula, M.F., et al. **(2017)** Local spin dynamics of iron oxide magnetic nanoparticles dispersed in different solvents with variable size and shape: A 1H NMR study, J Chem Phys. 146(3): 034703.

34. Lévy, M., Wilhelm, C., Devaud, M., Levitz, P., Gazeau, F.. **(2012)** How cellular processing of superparamagnetic nanoparticles affects their magnetic behavior and NMR relaxivity, Contrast Media Mol Imaging. 7(4): 373-83.

35. Baaziz, W., Pichon, B.P., Fleutot, S., Liu, Y., et al. **(2014)** Magnetic Iron Oxide Nanoparticles: Reproducible Tuning of the Size and Nanosized-Dependent composition, Defects, and Spin Canting| J. Phys. Chem. C 118: 3795−3810

36. Frey, N.A., Peng, S., Cheng, K. and Sun, S. (**2009**). "Magnetic nanoparticles: synthesis, functionalization, and applications in bioimaging and magnetic energy storage." Chemical Society Reviews 38(9): 2532-2542.

Accepted Manuscript

37. Kwon, S.G., Piao, Y., Park, J., Angappane, S., et al. (**2007**). "Kinetics of monodisperse iron oxide nanocrystal formation by "heating-up" process." Journal of the American Chemical Society 129(41): 12571-12584.

38. Cushing, B.L., Kolesnichenko, V.L. and O'Connor, C.J. (**2004**). "Recent advances in the liquid-phase syntheses of inorganic nanoparticles." Chemical Reviews 104(9): 3893-3946.

39. Kim, B.H., Lee, N., Kim, H., An, K., et al. (**2011**). "Large-scale synthesis of uniform and extremely small-sized iron oxide nanoparticles for high-resolution T_1 magnetic resonance imaging contrast agents." Journal of the American Chemical Society 133(32): 12624-12631.

40. Willard, M.A., Kurihara, L.K., Carpenter, E.E., Calvin, S., et al. (**2004**). "Chemically prepared magnetic nanoparticles." International Materials Reviews 49(3-4): 125-170.

41. LaMer, V.K. and Dinegar, R.H. (**1950**). Theory, production and mechanism of formation of monodispersed hydrosols. Journal of the American Chemical Society 72(11): 4847-4854.

42. Salas, G., Casado, C., Teran, F.J., Miranda, R., et al. (**2012**). Controlled synthesis of uniform magnetite nanocrystals with high-quality properties for biomedical applications. Journal of Materials Chemistry 22(39): 21065-21075.

43. Hoene, J.V., Charles, R.G. and Hickam, W.M. (**1958**). Thermal Decomposition of Metal Acetylacetonates: Mass Spectrometer Studies. The Journal of Physical Chemistry 62(9): 1098-1101.

44. Roch, A., Muller, R.N. and Gillis, P. (**1999**). Theory of proton relaxation induced by superparamagnetic particles. The Journal of Chemical Physics 110(11): 5403-5411.

45. Frenkel, J. and Doefman, J. (**1930**). Spontaneous and induced magnetisation in ferromagnetic bodies. Nature 126: 274-275.

46. Roch, A., Gillis, P., Ouakssim, A. and Muller, R.N. (**1999a**). Proton magnetic relaxation in superparamagnetic aqueous colloids: a new tool for the investigation of ferrite crystal anisotropy. Journal of Magnetism and Magnetic Materials 201(1-3): 77-79.

47. Laurent, S., Forge, D., Port, M., Roch, A., et al. (**2008**). Magnetic iron oxide nanoparticles: synthesis, stabilization, vectorization, physicochemical characterizations, and biological applications. Chemical Reviews 108(6): 2064-2110.

48. S. Laurent, C. Henoumont, D. Stanicki, S. Boutry, E. Lipani, S. Belaid, R.N. Muller, L. Vander Elst, **(2017)** MRI Contrast Agents: From Molecules to Particles, Springer Series "Briefs in Applied Sciences and Technology – Nanotheranostics", DOI 10.1007/978-981-10-2529-7, Springer-Nature, Singapore, Singapore

49. Moore, J.W. and Wellek, R.M. (**1974**). Diffusion coefficients of n-heptane and n-decane in n-alkanes and n-alcohols at several temperatures. Journal of Chemical & Engineering Data 19(2): 136-140.

Accepted Manuscript

50. Laurent, S., Bridot, J.-L., Vander Elst, L. and Muller, R.N. (**2010**). Magnetic iron oxide nanoparticles for biomedical applications. Future Medicinal Chemistry 2(3): 427-449.

51. Freed, J.H. (**1978**). Dynamic effects of pair correlation functions on spin relaxation by translational diffusion in liquids. II. Finite jumps and independent T[sub 1] processes. The Journal of Chemical Physics 68(9): 4034-4037.

52. Belaïd, S., Laurent, S., Vermeersch, M., Vander Elst, L., et al. (**2013**). A new approach to follow the formation of iron oxide nanoparticles synthesized by thermal decomposition. Nanotechnology 24(5): 055705.

53. D'Agostino, A.T. (**1992**). Determination of thin metal film thickness by x-ray diffractometry using the Scherrer equation, atomic absorption analysis and transmission/reflection visible spectroscopy. Analytica Chimica Acta 262(2): 269-275.

54. Demortiere, A., Panissod, P., Pichon, B.P., Pourroy, G., et al. (**2011**). Size-dependent properties of magnetic iron oxide nanocrystals. Nanoscale 3(1): 225-232.

55. Schladt, T.D., Graf, T. and Tremel, W. (**2009**). Synthesis and characterization of monodisperse manganese oxide nanoparticles−evaluation of the nucleation and growth mechanism. Chemistry of Materials 21(14): 3183-3190.

56. Maity, D., Ding, J. and Xue, J.-M. (**2008**). Synthesis of magnetite nanoparticles by thermal decomposition: time, temperature, surfactant and solvent effects. Functional Materials Letters 1(3): 189-193.

57. Teng, X. and Yang, H. (**2004**). Effects of surfactants and synthetic conditions on the sizes and self-assembly of monodisperse iron oxide nanoparticles. Journal of Materials Chemistry 14(4): 774-779.

58. Yin, M., Willis, A., Redl, F., Turro, N.J., et al. (**2004**). Influence of capping groups on the synthesis of alpha-Fe_2O_3 nanocrystals. Journal of Materials Research 19(4): 1208-1215.

59. Bronstein, L.M., Atkinson, J.E., Malyutin, A.G., Kidwai, F., et al. (**2011**). Nanoparticles by decomposition of long chain iron carboxylates: from spheres to stars and cubes. Langmuir 27(6): 3044-3050.

60. Guardia, P., Batlle-Brugal, B., Roca, A.G., Iglesias, O., et al. (**2007**). Surfactant effects in magnetite nanoparticles of controlled size. Journal of Magnetism and Magnetic Materials 316(2): e756-e759.

61. Zhu, Y., Jiang, F.Y., Chen, K., Kang, F., et al. (**2011**). Size-controlled synthesis of monodisperse superparamagnetic iron oxide nanoparticles. Journal of Alloys and Compounds 509(34): 8549-8553.

62. Crouse, C.A. and Barron, A.R. (**2008**). Reagent control over the size, uniformity, and composition of Co-Fe-O nanoparticles. Journal of Materials Chemistry 18(35): 4146-4153.

563. Vargas, J.M. and Zysler, R.D. (**2005**). Tailoring the size in colloidal iron oxide magnetic nanoparticles. Nanotechnology 16(9): 1474.

Accepted Manuscript

64. Meledandri, C.J., Stolarczyk, J.K., Ghosh, S. and Brougham, D.F. (**2008**). Nonaqueous magnetic nanoparticle suspensions with controlled particle size and nuclear magnetic resonance properties. Langmuir 24(24): 14159-14165.

65. Bronstein, L.M., Huang, X., Retrum, J., Schmucker, A., et al. (**2007**). Influence of iron oleate complex structure on iron oxide nanoparticle formation. Chemistry of Materials 19(15): 3624-3632.

Accepted Manuscript